25th ABCM International Congress of Mechanical Engineering
October 20-25, 2019, Uberlândia, MG, Brazil

COB-2019-1516
NUMERICAL EVALUATION OF A DIFFUSIVE MODEL FOR Sn - 39.5 wt% Bi ALLOY SOLIDIFICATION EXPERIMENT

Leonardo Maximino Bernardo
Programa de Pós-Graduação em Ciência e Engenharia de Materiais/UFPB
lmbernardo752011@gmail.com

Romulo Heringer
Universidade Federal de Santa Catarina
romulo.heringer@ufsc.br

Abstract. *The present contribution is a numerical simulation for a solidification experiment of Sn - 39.5 wt% Bi alloy, performed by others, who used in-situ X-ray radiography to observe microstructures during their growth. Heat and solute transfers, phase change and dendrite growth kinetic were evaluated in order to analyze: a) if recalescence occurs which could contribute to the fragmentation rate observed in the experiment; b) the contribution, for the solid fraction evolution, of the remelting associated with diffusion caused by differences on the curvature of dendrites arms interface. We proposed a mathematical model elaborated for the solidification of Sn - 39.5 wt% Bi which allowed us to evaluate the questions stated above. We found that, including the remelting mentioned above in the solid fraction calculation leads to better agreement, when compared to data reported in the literature related to the concerned experiment.*

Keywords: *solidification, numerical modeling, heat and mass transfer.*

1. INTRODUCTION

Metal alloys with a refined grain structure are associated with higher mechanical properties. Spontaneous grain refining, which means one that occurs naturally in the material and does not come from the addition of inoculants, had been observed first by Walker (1959) and continues to be a targeted objective in research on solidification processes. Since the experiments carried out by Jackson (1966), it is generally reported that spontaneous grain refinement has a determining cause in dendrites fragmentation. In recent models there seems to be a consensus that the mechanisms of fragmentation by remelting followed by the coarsening of the dendritic fragments are at the origin of the spontaneous grain refining. Schwarz *et al.* (1994) and then Karma (1998) have proposed models to predict grain refinement where they adopt as the trigger mechanisms for this phenomenon a sequence of events: fragmentation and buoyancy or advection of these detached dendrite branches, followed by a process driven by surface tension where the branches assume a near spherical shape. This last particles act as nucleation sites for grain refinement.

However, it's still in debate the mechanism of remelting behind this fragmentation phenomenon. Several mechanisms supported by experimental observations have been proposed, among which we can mention the coarsening, solute enrichment, solute redistribution and recalescence (Ruvalcaba *et al.* (2007), Abdelaziz *et al.* (2017)).

Gibbs *et al.* (2016) performed *In-situ* visualization experiments of the solidification of a Sn - 39.5 wt% Bi alloy, using an apparatus detailed in Clarke *et al.* (2017). Their aim was to evaluate the amount of fragmentation in two specific experiments: top-down and bottom-up solidification.

The aim of the present model is to evaluate the heat and solute transfer in the experiment of Gibbs *et al.* (2016), searching for possible remelting cause which could be associated with the amount of fragmentation observed by them. Specifically, in this work we deal with two issues: first, if recalescence occurs which could contribute to the fragmentation rate observed in the experiment; second, if the solid fraction evolution is affected by the remelting associated with dendrite secondary arms evolution, as described in the literature related to coarsening (Dantzig and Rappaz (2009)).

2. NUMERICAL MODELING OF Sn - 39.5 wt% Bi ALLOY SOLIDIFICATION PROCESS

2.1 Preliminary analysis of thermal conditions in the experiment

In order to establish the control volume, as well as the initial and boundary conditions for the solidification model, a preliminary analysis of heat transfer on the experimental device was carried out. Figure 1 schematically indicates the control volume used on this task. Considering symmetry related to a middle plane, the control volume of the Fig. 1 represents a half part of a longitudinal cutting of the device and consists of a two-dimensional area with two subregions and, for each of them, thermal properties for steel (furnace material) and for boron (crucible material) have been assigned. With suitable simplifications the problem was reduced to transient two-dimensional heat conduction. The amount of enthalpy of fusion associated to the solidification of entire sample along time was introduced via boundary condition as a heat flux q''.

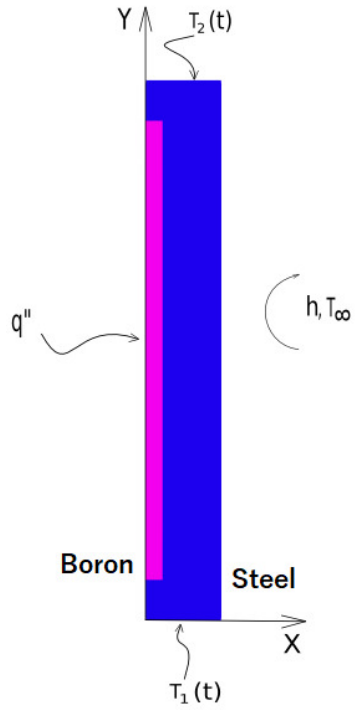

Figure 1. Schematic view of the control volume used in the auxiliary model.

The results obtained from this previous analysis show that the thermal gradient remains constant along the longitudinal direction of the device, in the furnace and the crucible, throughout the process, even in regions close to the sample. These results allowed to establish the control volume, the initial and boundary conditions for the solidification model. In the next sections we present this model.

2.2 Control volume and further hypothesis for the directional solidification model

For the present model, the following considerations was made: a) based on the previous analysis, as shown in the Fig. 2, the control volume consists of a rectangle limited longitudinally by the sample length and transversely by the half width of the device, due to symmetry; b) the control volume is divided in three subregions (sample alloy, crucible (boron) and furnace (steel); c) the thermal properties are mapped for each material inside the control volume and the solid fraction on crucible and furnace regions are always equal one (solid); d) the sample region is initially fully liquid; e) the solidification start on the coldest face at a given undercooling; d) the initial undercooling is chosen in order to fit the front velocity data of the reference Gibbs *et al.* (2016) (see section 4.1); e) during solidification, a front tracking technique allows to distinguish the liquid region from the mushy zone; c) there is no convection caused by thermal or solutal gradients in the liquid alloy.

2.3 Heat transfer

We defined the conservation equations for thermal energy in their integral average form, invoking the condition that the intrinsic average values of temperature in solid and liquid phases inside a representative

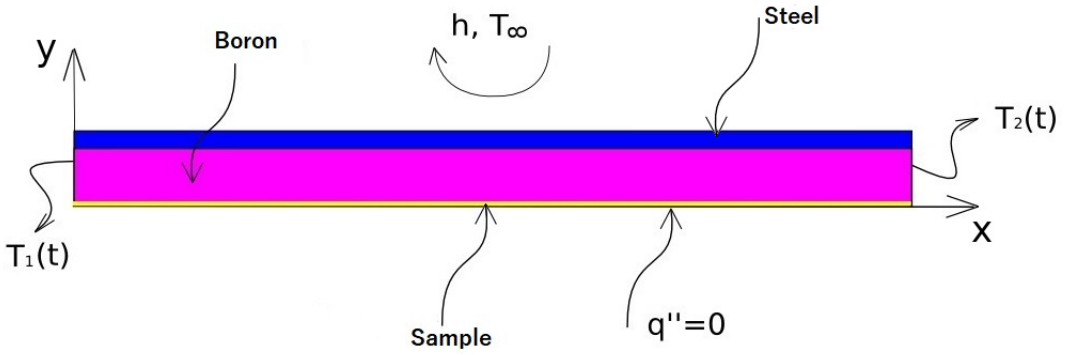

Figure 2. Schematic view of the control volume used for solidification.

small volume of reference are equal, resulting in the following equation

$$\frac{\partial}{\partial t}\langle \rho h \rangle = -\boldsymbol{\nabla} \cdot (\langle \kappa \rangle \, \boldsymbol{\nabla} T) \tag{1}$$

where the angle brackets "$\langle\ \rangle$" denotes a volumetric average of a property in a solid liquid mixture; h is the specific enthalpy; κ is the thermal conductivity. The average enthalpy and the average specific heat was written as

$$\langle H \rangle = \langle c \rangle \, T + (1 - g_s) L \tag{2}$$

where g_s is the volumetric solid fraction. L is the enthalpy of fusion, and $\langle c \rangle$ is the mean specific volumetric heat of the solid/liquid mixture, $\langle c \rangle = g_s c_s + (1 - g_s) c_\ell$. Particularly, the specific volumetric heats of the solid, c_s, and liquid phases, c_ℓ, will be considered equal to the mean value $\langle c \rangle$.

For the thermal problem the initial and boundary conditions, after taking the averages are:

$$-\langle k \rangle \frac{\partial T}{\partial x} = 0; \ \text{ para : } \ 0 \leq x \leq 30.0 \times 10^{-3}\,\text{m}; \ y = 0 \tag{3}$$

$$-\langle k \rangle \frac{\partial T}{\partial x} = h_c (T_{N0} - T_\infty); \ \text{ para : } \ 0 \leq x \leq 30.0 \times 10^{-3}\,\text{m}; \ y = 2.0 \times 10^{-3}\,\text{m} \tag{4}$$

$$T(x, y, t) = T_{L0} + \left(\frac{dT}{dt}\bigg|_L \right) t; \ \text{ para : } \ x = 0; \ 0 \leq y \leq 2.0 \times 10^{-3}\,\text{m} \tag{5}$$

$$T(x, y, t) = T_{O0} + \left(\frac{dT}{dt}\bigg|_O \right) t; \ \text{ para : } \ x = 30.0 \times 10^{-3}\,\text{m}; \ 0 \leq y \leq 2.0 \times 10^{-3}\,\text{m} \tag{6}$$

With T_{L0} and T_{O0} being the initial temperatures on the indicated faces. $\left(\frac{dT}{dt}\Big|_{L0} \right) = \left(\frac{dT}{dt}\Big|_{O0} \right) = -0.06033\,\text{Ks}^{-1}$ corresponding to the imposed temporal rate of temperature.

2.4 Solute transfer

The average balance equation of solute in terms of the average mass fraction, $\langle w \rangle$. $\langle w_\ell \rangle^\ell$, is the intrinsic average mass fraction of solute in the liquid, such that $\langle w_\ell \rangle^\ell = g_s \, \langle w \rangle$. D_ℓ is the solute diffusivity coefficient in the liquid.

$$\frac{\partial}{\partial t}\langle w \rangle = \boldsymbol{\nabla} \cdot [(1 - g_s) D_\ell \boldsymbol{\nabla} \langle w_\ell \rangle^\ell] \tag{7}$$

And the initial and boundary conditions, for the mass problem, after taking the average are:

$$\frac{\partial \langle w \rangle}{\partial x} = 0; \text{ para : } 0 \leq x \leq 30.0 \times 10^{-3}\,\text{m}; \; y = 0 \tag{8}$$

$$\frac{\partial \langle w \rangle}{\partial x} = 0; \text{ para : } 0 \leq x \leq 30.0 \times 10^{-3}\,\text{m}; \; y = 2.0 \times 10^{-3}\,\text{m} \tag{9}$$

$$\frac{\partial \langle w \rangle}{\partial y} = 0; \text{ para : } x = 0; \; 0 \leq y \leq 2.0 \times 10^{-3}\,\text{m} \tag{10}$$

$$\frac{\partial \langle w \rangle}{\partial y} = 0; \text{ para : } x = 30.0 \times 10^{-3}\,\text{m}; \; 0 \leq y \leq 2.0 \times 10^{-3}\,\text{m} \tag{11}$$

2.5 Local phase equilibrium

We use the phase equilibrium diagram to calculate the mass concentrations at the interface on the solid side, $w^{s\ell}$, and on the liquid side, $w^{\ell s}$, at local temperature. The *liquidus* line in the phase diagram are usually represented by n-degree polynomial:

$$T^{\ell s} = T_f + \sum_{i=1}^{N} [m_{\ell i} (w^{\ell s})^i] \tag{12}$$

Where, if a linear approximation is made, each $m_{\ell i}$ is the slope of the *liquidus* line for the component i. $T^{\ell s}$ and $T^{s\ell}$ being the temperature at solid-liquid interface, respectively on the liquid and solid sides, the local thermodynamic equilibrium among the phases impose that $T^{s\ell} = T^{\ell s} = T$. The *solidus* line is found by defining a partition coefficient, k_0, such that

$$w^{s\ell} = k_0\, w^{\ell s}$$

If the temperature of the eutectic point is reached and the eutectic reaction is triggered, then the mass composition near the liquid side interface will be considered equal to the eutectic composition, w_E. We will mathematically characterize the permanence of the system in the eutectic phase while the average enthalpy value is greater than the product of the volumetric specific heat of the solid by the temperature in the eutectic.

2.6 Solid fraction

The solid fraction calculation was based on the microsegregation model of Gulliver-Scheil expressed by

$$g_{sS} = 1 - \left(\frac{w^{\ell s}}{w_0} \right)^{1/(k_0 - 1)} \tag{13}$$

where g_{sS} denotes here the solid fraction done by Gulliver-Scheil model and w_0 is the nominal solute concentration.

However, in the present work we had proposed to take into account the amount of solid remelted associated to coarsening process. In the next section this will be discussed in detail. For now, let us denote by Δg_{sc} this reduction on solid fraction during a time step Δt. So the solid fraction g_s would be done by

$$g_s = g_{sS} + \Delta g_{sc} \tag{14}$$

During eutectic transformation, the variation of solid fraction is directly related to the variation of the average enthalpy value, being written as:

$$dg_s = -\frac{1}{L} d \langle \rho h \rangle \tag{15}$$

2.7 Remelting associated to dendrite arms coarsening

Coarsening is a phenomenon that occurs on the length scale of microstructures which consists of elimination of certain dendrites branches and growth of others. This mechanism is associated to diffusion of solute caused by difference in curvature of the solid-liquid interface. Branches with larger curvature lost solute and

tends to redissolve in liquid. This process continues until a final dendritic secondary arms spacing is reached. It is believed also to be at the origin of dendrite fragmentation (Schwarz *et al.* (1994), Herlach (1994)).

Kattamis and Flemings (1970) have developed a model that explains the phenomenon by identifying its significant parameters. The model is restricted to three neighboring and adjacent branches, designed as cylinders that evolve with different radii, R and r, separated by an initial secondary dendritic spacing λ_2^0. The temperature is assumed to be uniform over the length scale of the elemental volume containing the cylinders, and the solid and hot liquid are in thermodynamic equilibrium. The Gibbs-Thomson equation implies that the concentration in the liquid must be different on the surfaces of the neighboring dendritic arms because they are the same temperature but have different radii of curvature. Let us denote the concentration at the interface of the major arm as $w_R^{\ell s}$ and for the minor arm as $w_r^{\ell s}$. This arrangement results in a concentration gradient, and consequently a flow of solute. To reach the local equilibrium, the solid that lost solute becomes overheated in relation of local *liquidus* temperature and remelts while the larger dendritic arm increases. As a result the difference between dendritic arm compositions, $\left(w_R^{\ell s} - w_r^{\ell s}\right)$, also increases. The process continues until the smaller arm completely fades or fragments.

Assuming the concentration profile to be linear between two neighboring arms, a one-dimensional treatment of diffusion results in an equation for flow in liquid given by:

$$j = -D_\ell \frac{\partial w_\ell}{\partial x} \approx D_\ell \frac{\left(w_R^{\ell s} - w_r^{\ell s}\right)}{\lambda_2^0} \tag{16}$$

Taking the slope of the *liquidus* curve to be constant, and equaling the temperature of both cylinders, we get the result.

$$T_f + m_\ell\, w_R^{\ell s} - \frac{\Gamma_{s\ell}}{R} = T_f + m_\ell\, w_r^{\ell s} - \frac{\Gamma_{s\ell}}{r} \tag{17}$$

With $\Gamma_{s\ell}$ being the Gibbs-Thomson coefficient, the ratio of interfacial energy $\gamma_{s\ell}$ to fusion entropy variation (ΔS_f). Resolving for $\left(w_R^{\ell s} - w_r^{\ell s}\right)$ and overriding in 16

$$j = -\frac{D_\ell\, \Gamma_{s\ell}}{m_\ell\, \lambda_2^0} \left(\frac{1}{r} - \frac{1}{R}\right) \tag{18}$$

This solute flow dissolves the smaller dendritic arm at a rate that can be calculated from the flow balance at the interface:

$$\frac{dr}{dt} = \frac{D_\ell\, \Gamma_{s\ell}}{m_\ell\, \lambda_2^0\, (1 - k_0)\, w_r^{\ell s}} \left(\frac{1}{r} - \frac{1}{R}\right) \tag{19}$$

In this model the larger arm is assumed to remain approximately constant, which is not necessarily inconsistent if $R \gg r$, Mortensen (1991).

It is proposed here that coarsening remelting should be taken into account when calculating the solid fraction. This proposal is based on the hypothesis that the influence of the volume of solid remelted by coarsening may not be negligible in the calculation of the solid fraction. Note however that even if there is local remelting, the solid fraction may be increasing depending on the intensity of solidification. To account for this dissolution in calculating the solid fraction, we start from Eq. (19).

The intermediate cylinder volume (dendritic radius r) and its time derivative are calculated as

$$V_c = \pi r^2 \frac{\lambda_1}{2} \quad \Rightarrow \quad \frac{dV_c}{dt} = \pi \lambda_1 r \frac{dr}{dt} \tag{20}$$

The solid fraction of the intermediate cylinder g_{sc} is given by the ratio of the volume of the solid V_c to the domain V_R.

$$g_{sc} = \frac{V_c}{V_R} \tag{21}$$

Taking the time derivative of the Eq. (21),

$$\frac{dg_{sc}}{dt} = \frac{1}{V_R} \frac{dV_c}{dt} = \frac{1}{V_R} \pi\, \lambda_1\, r\, \frac{dr}{dt}$$

and using Eq. (20) and Eq. (19), we obtain, after recognizing that $w_r^{\ell s} = w^{\ell s}$,

$$\frac{dg_{sc}}{dt} = \frac{3\,D_\ell\,\Gamma_{s\ell}}{V_R\,\lambda_2\,m_\ell\,w^{\ell s}\,(1-k_0)}\left(1-\frac{2^{\frac{3}{2}}}{\lambda_2}\sqrt{\frac{g_s\,V_R}{\pi\lambda_1}}\right) \tag{22}$$

One could argue that while the vanishing arms remelts, other arms grow associated to the same coarsening process. Therefore, this should compensate the remelting and Δg_{sc} should be unnecessary. However, this is not the case, because the solid growth is already taken into account in Gulliver-Scheil equation.

3. NUMERICAL APPROACH

In this work we have applied an algorithm for the numerical resolution of solidification problems which details can be found in Heringer (2004) and Heringer *et al.* (2006). The only exception is that the microsseg-regation model used in these references was the Gulliver-Scheil equation. In the present work we propose an additional term, noted at Eq. (14), where Δg_{sc} is the amount of coarsening remelting during a time interval Δt and is determined by

$$\Delta g_{sc} = \frac{dg_{sc}}{dt}\,\Delta t \tag{23}$$

The term $\frac{dg_{sc}}{dt}$ is solved numerically, by using on the right side of Eq. (22) an $g_s(t+\Delta t)$ available from previous numerical interaction. By coarsening remelting, referred here, we mean the remelting associated to the diffusion by curvature differences, which, in turn, is related to dendrite arm spacing evolution, as discussed in section 2.7.

4. RESULTS AND DISCUSSIONS

Our general conditions for calculating the equations of the model take into account a value for the undercooling in the nucleus of the first crystal of $\Delta T_N = 8\,\mathrm{K}$. The other parameters are, the size of the control volume, $(30.0\times10^{-3}\,\mathrm{m})\times(2.0\times10^{-3}\,\mathrm{m})$, the initial composition of the sample is Sn - 39.5 wt% Bi , and the heat transfer coefficient to the outside, $h_c = 9.4\,\mathrm{Wm^{-2}K^{-1}}$.

4.1 Initial undercooling

For the numerical and experimental results to be comparable, it should be noted that the experimental measurements were all taken in a small region in the middle of the sample. Nothing is known quantitatively about what occurs outside this visible region. It is not known how long it takes from the beginning of solidification until the solid appears in the visible area. Indeed, it cannot be stated with certainty where solidification began, although it is an experiment intended to achieve directional bottom-up solidification.

In order to compare our numerical results with the experimental data, the curves of solidification velocity calculated for various undercoolings were simultaneously shifted horizontally (time translation), until the slope of the curves (rate of change of the solidification velocity) were satisfactorily represented. We then chose the curve whose values fit the best possible with the experimental data. From the Fig. 3, the undercooling value $\Delta T_N = 8\,\mathrm{K}$ was chosen as best representing the experimental values. This procedure allows to evaluate an initial undercooling. This information is not immediately available from the experiments.

4.2 Evolution of temperature

The results of present model show that temperature profiles at transverse sections of the device are nearly uniforms, despite the enthalpy of fusion liberated during solidification. In addition, the thermal gradient along a longitudinal device axis remains constant as shown in Fig. 4, where can be observed that the temperature intervals between the curves do not change over time. This is due to small sample volume compared to the surrounding materials. These results show that there is no recalescence that could be the origin of remelting.

4.3 Evolution of averaged solid fraction

Figure 5 shows numerical results along with experimental data for the evolution of solid fraction measured by Gibbs *et al.* (2016). These experimental measurements were performed by analysis of images obtained by x-ray radiography trough a small region of the sample. To be coherent with experimental data, the numerical solid fraction curves of the Fig. 5 are averages of g_s field along a region comparable with the measurement window.

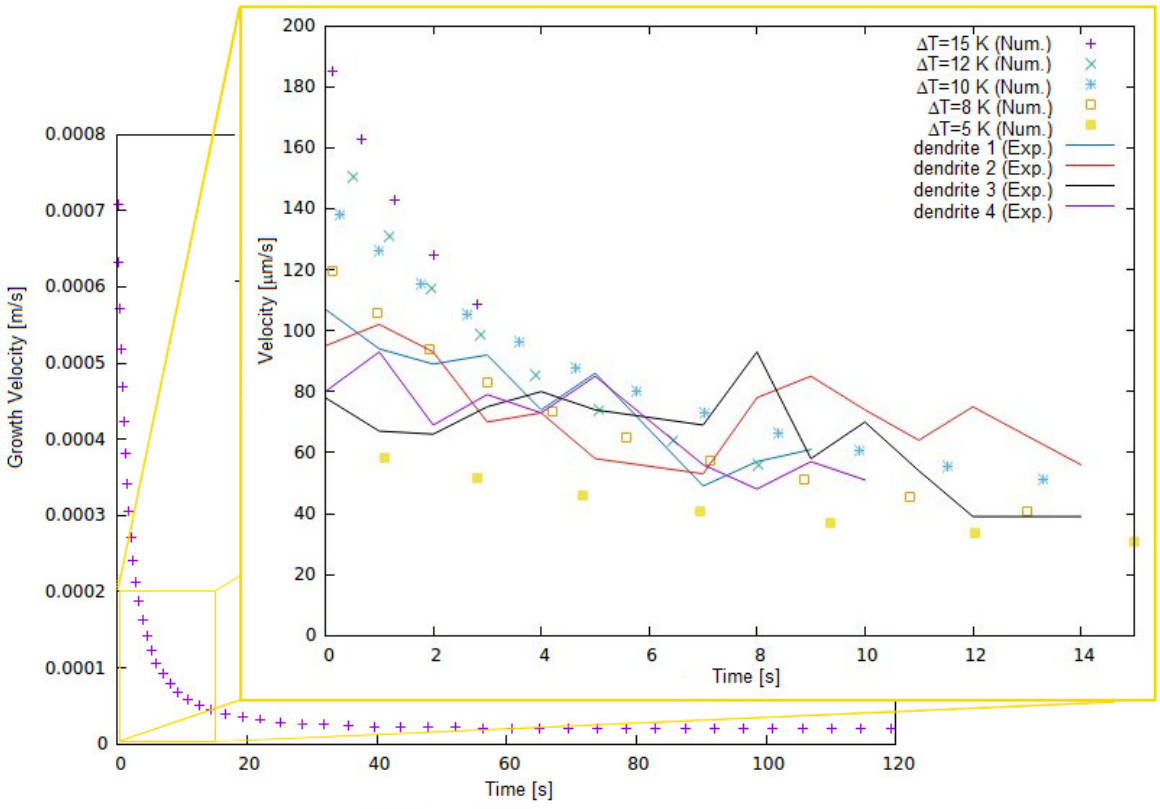

Figure 3. Choosing criteria for initial undercooling. The bottom graph is the result of the 8 K undercooling model until it reaches steady growth. The highlighted graph shows the numerical growth velocities calculated compared to the experimental measurements of four dendrite velocities in the experiment of Gibbs *et al.* (2016).

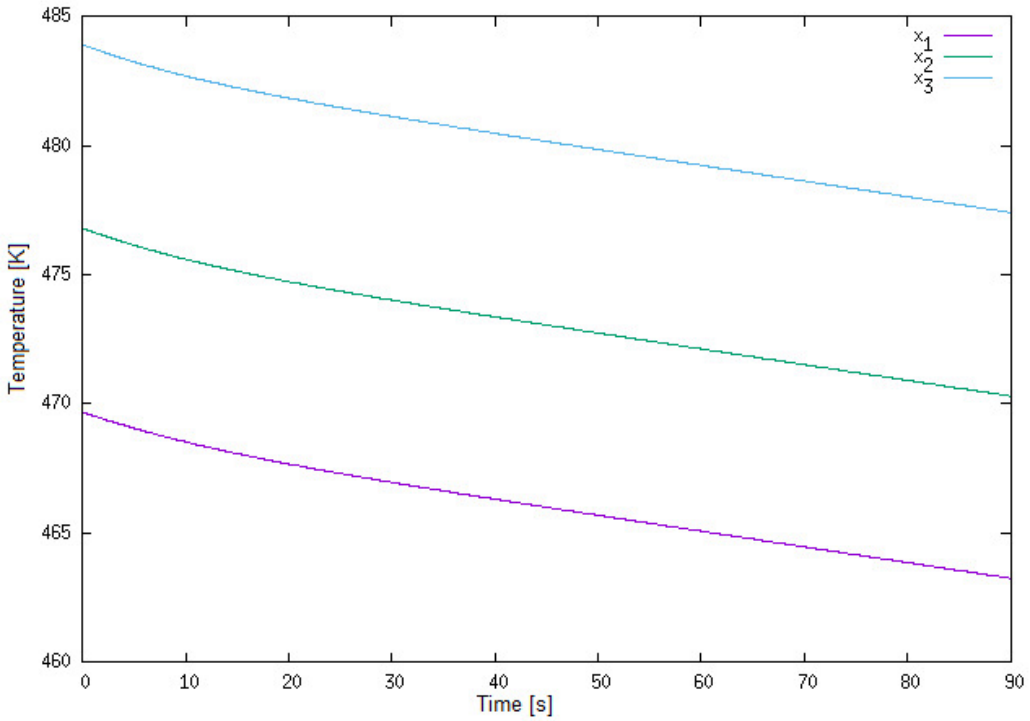

Figure 4. Temperature histories in positions $x_1 = 1.25 \times 10^{-2}$ m (magenta), $x_2 = 1.50 \times 10^{-2}$ m (green), $x_3 = 1.75 \times 10^{-2}$ m (cyan), for a initial undercooling $\Delta T = 8$ K.

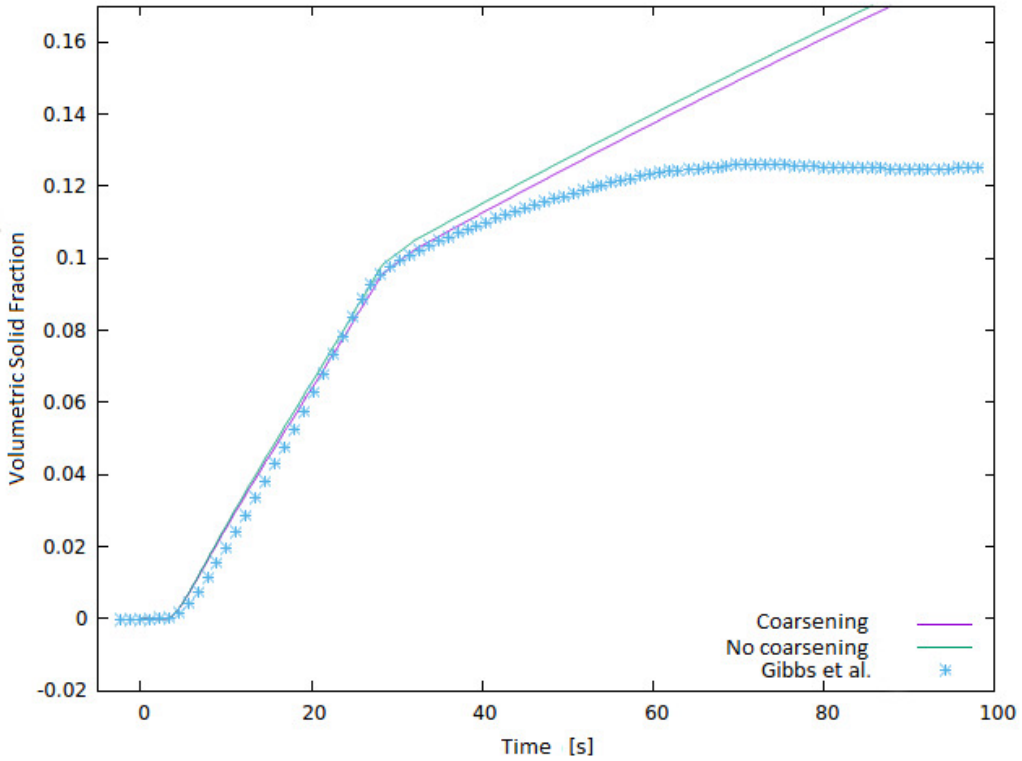

Figure 5. Time evolution of the volumetric average of solid fraction considering remelting with and without remelting associated to coarsening.

It shall be noted that the decreasing in the solid fraction observed in the experimental data was not due to remelting, but to buoyancy of dendrite fragments out of the measuring region. The results of the present model together with an image analysis allowed us to make this last conclusion, about which Gibbs *et al.* (2016) did not report in their paper. This local effect isn't included in the present model. So, no comparisons can be expected after this buoyancy effect becomes important.

Despite this fact, it can be noted a better agreement of the numerical results including remelting by coarsening effects with the experimental data, when compared with Gulliver-Scheil results (no coarsening).

5. CONCLUSIONS

A numerical model has been proposed for analysis of heat and solute diffusion of solidification of a Sn - 39.5 wt% Bi alloy. This model was applied to a specific experimental conditions described in Gibbs *et al.* (2016) and in Clarke *et al.* (2017). The results of this model allows to conclude that there is no recalescence in the sample solidified under the conditions cited. So, recalescence can not be associated to remelting at origin of fragmentation measured in the experiment.

On the other hand, it was calculated the amount of remelting associated with diffusion caused by differences on the curvature of dendrites arms interface. This remelting mechanism, which causes redissolution in liquid of some dendrite arms, a phenomenon closed related with fragmentation, is normally not taken into account in the calculation of solid fraction. However, the present results show that a measurable contribution exist in this context.

6. ACKNOWLEDGEMENTS

L. M. Bernardo is thankful to CAPES (Coordenação de Aperfeiçoamento de Pessoal de Nível Superior) for partial support of this work.

7. REFERENCES

Abdelaziz, S.M., Zahran, H. and El-Rehim, A.A., 2017. "Microstructure and mechanical properties of tin-bismuth solder alloy reinforced by antimony oxide nanoparticles". *International Journal of Advances in Engineering & Technology*, Vol. 10, No. 1, p. 73.

Clarke, A.J., Tourret, D., Song, Y., Imhoff, S.D., Gibbs, P.J., Gibbs, J.W., Fezzaa, K. and Karma, A., 2017. "Microstructure selection in thin-sample directional solidification of an al-cu alloy: in situ x-ray imaging and phase-field simulations". *Acta Materialia*, Vol. 129, pp. 203–216.

Dantzig, J.A. and Rappaz, M., 2009. *Solidification*. EPFL press.

Gibbs, J.W., Tourret, D., Gibbs, P.J., Imhoff, S.D., Gibbs, M.J., Walker, B.A., Fezzaa, K. and Clarke, A.J., 2016. "In situ x-ray observations of dendritic fragmentation during directional solidification of a sn-bi alloy". *JOM*, Vol. 68, No. 1, pp. 170–177.

Heringer, R., Gandin, C.A., Lesoult, G. and Henein, H., 2006. "Atomized droplet solidification as an equiaxed growth model". *Acta Materialia*, Vol. 54, No. 17, pp. 4427 – 4440. ISSN 1359-6454.

Heringer, R., 2004. *Modélisation de la solidification de gouttes atomisées*. Ph.D. thesis, INPL, Nancy, France.

Herlach, D.M., 1994. "Non-equilibrium solidification of undercooled metallic metls". *Materials Science and Engineering: R: Reports*, Vol. 12, No. 4-5, pp. 177–272.

Jackson, K. A. Hunt, J.D.U.D.R.S.T.P., 1966. "On the origin of the equiaxed zone in castings". *Transactions of the Metallurgical Society of AIME*, pp. 149–158.

Karma, A., 1998. "Model of grain refinement in solidification of undercooled melts". *International Journal of Non-Equilibrium Processing*, Vol. 11, pp. 201–233.

Kattamis, T. and Flemings, M., 1970. "Structure of undercooled ni-sn eutectic". *Metallurgical and Materials Transactions*, Vol. 1, No. 5, pp. 1449–1451.

Mortensen, A., 1991. "On the rate of dendrite arm coarsening". *Metallurgical Transactions A*, Vol. 22, No. 2, pp. 569–574.

Ruvalcaba, D., Mathiesen, R., Eskin, D., Arnberg, L. and Katgerman, L., 2007. "In situ observations of dendritic fragmentation due to local solute-enrichment during directional solidification of an aluminum alloy". *Acta Materialia*, Vol. 55, No. 13, pp. 4287–4292.

Schwarz, M., Karma, A., Eckler, K. and Herlach, D.M., 1994. "Physical mechanism of grain refinement in solidification of undercooled melts". *Physical Review Letters*, Vol. 73, pp. 1380–1383. doi: 10.1103/PhysRevLett.73.1380. URL `https://link.aps.org/doi/10.1103/PhysRevLett.73.1380`.

Walker, J.L., 1959. "The influence of large amounts of undercooling on the grain size of nickel". In G.R. St. Pierre, ed., *The Physical Chemistry of Process Metallurgy*, Interscience, New York, pp. 845–853.

8. RESPONSIBILITY NOTICE

The authors are the only responsible for the printed material included in this paper.